Supporting Information

Sitia et al. 10.1073/pnas.1209182109

SI Materials and Methods

Disease Models. The mouse model of immune-mediated chronic hepatitis consists of hepatitis B virus (HBV) transgenic (TG) mice (lineage 107-5, inbred B10D2) in which 100% of the hepatocytes express nontoxic quantities of the HBV large, middle, and small envelope proteins [all containing hepatitis B surface antigen (HBsAg) determinants] (1). Lineage 107-5 mice are immunologically tolerant to HBsAg and spontaneously develop neither chronic hepatitis nor hepatocellular carcinoma (HCC) unless their immune system is destroyed (by thymectomy and irradiation) and replaced by sequentially infusing nontransgenic (NTG) B10D2 bone marrow (BM) cells and spleen cells from B10D2 mice that had been immunized to produce an HBsAg-specific $CD8^+$ T-cell response (1, 2). The 8- to 10-wk-old male TG mice (n = 430) were thymectomized as described (1). Seven days later, the mice were irradiated (1,100 cGy) and immediately reconstituted with either NT or TG B10D2 BM as described (1). Seven days later, 10^8 spleen cells from NT B10D2 mice that had been immunized at least 2 mo earlier with plasmid DNA- (prime) and vaccinia virus-encoding HBsAg (boost) as described (3, 4) were adoptively transferred into the mice that had received NT BM (n = 320) (1, 2). Simultaneously, the mice that had received TG BM were injected with 10^8 spleen cells from nonimmunized TG 107-5 littermates (n = 110). A final group of 110 male TG mice [control (Ctrl)] remained unmanipulated for the entire experiment for baseline comparison.

The mouse model of carbon tetrachloride (CCl_4)-induced chronic hepatitis was adapted from Jang et al. (5). Briefly, 8- to 10-wk-old male 107-5 mice were fed by oral gavage with a solution of CCl_4 (Sigma–Aldrich) in peanut oil (Sigma–Aldrich) at a final dose of 0.7 mg/g of body weight. CCl_4 was administered twice a week for 16 wk, after which the treatment was suspended for a washout period of ∼30 wk.

Blood Analyses. Serum alanine aminotransferase activity was measured with an International Federation of Clinical Chemistry and Laboratory Medicine optimized kinetic UV method in a SABA chemical analyzer (Seac–Radim), and it is expressed as units per liter. Complete cell counts were measured in whole blood collected in 1/10th volume of citrate phosphate dextrose (Sigma–Aldrich) using an automated cell counter (HeCoVet; Seac–Radim). Platelet aggregation analysis was performed on platelet-rich plasma prepared as described (6). Aggregation was induced by the addition of ADP (Mascia Brunelli) at a final concentration of 2.5 μM and monitored continuously by recording changes in light transmittance through the stirred platelet suspension. The platelet thromboxane ($TX\text{-}A_2$)-forming capacity was evaluated by measuring the serum content of the stable metabolite $TX\text{-}B_2$, thanks to a commercially available enzyme immunoassay (Thromboxane B_2 EIA Kit; Cayman Chemical Company) according to the manufacturer's instructions.

Liver Histopathology. At the time of autopsy, six or more different liver pieces per mouse were collected, fixed in Zn-formalin, and processed for H&E or Sirius Red staining as described (4). Visible macroscopic tumors were sectioned and fixed separately. Two pathologists independently analyzed liver sections in a blinded fashion and used a semiquantitative Ishak-based (7) scoring system to grade necroinflammatory activity and stage fibrosis. Each necroinflammatory parameter [(*i*) piecemeal necrosis; (*ii*) confluent necrosis; (*iii*) focal lytic necrosis, apoptosis, and focal inflammation; and (*iv*) portal inflammation] was added to generate four different categories of liver disease (none, mild, moderate, or severe). Liver fibrosis was staged after Sirius Red staining, and it was classified as follows: F0, no fibrosis; F1, fibrous expansion of some portal areas with or without short fibrous septa; F2, fibrous expansion of most portal areas with or without short fibrous septa; F3, bridging fibrosis without cirrhosis; and F4, cirrhosis with architectural distortion. Immunohistochemical analyses for HBsAg, Ki67, collagen type I, and CD34 were performed as described (8). Quantification of liver collagen deposition and hepatocellular regeneration was performed by calculating the extent of Sirius Red, collagen type I, and Ki67 staining through an Aperio Scanscope System XT microscope and an ImageScope program (Aperio Technologies, Inc.) following the manufacturer's instructions.

Analyses of the Cellular Immune Response. Leukocyte isolation from liver, spleen, or portal lymph nodes was performed as described (4). Cells were surface-stained with phycoerythrin (PE)-conjugated anti-CD4 (clone RM4-5; BD Pharmingen) and anti-CD11c (clone HL3; BD Pharmingen), Pacific Blue-conjugated anti-CD8 (clone 53-6.7; BD Pharmingen) and anti-CD3 (clone 145-2c11; BD Pharmingen), PE-Cy7–conjugated anti-CD11b (clone M1/70; BD Pharmingen), allophycocyanin-conjugated anti–T-cell receptor (TCR; clone H57-597; BD Pharmingen), and anti-Ly6G (clone 1A8; BD Pharmingen) for the detection of $CD8^+/TCR^+$ cells ($CD8^+$ T cells), $CD4^+/TCR^+$ cells (T helper cells), $LY6G^+/CD11c^-$ cells (neutrophils), $CD11b^-/CD11c^+$ cells (dendritic cells), $CD11b^+/CD11c^-$ cells (macrophages), $NK1.1^+/CD3^-$ cells [natural killer (NK) cells] and $NK1.1^+/CD3^+$ cells (NKT cells). HBsAg-specific $CD8^+$ T cells were quantified by staining intrahepatic leukocytes (IHLs) with Pacific Blue-conjugated anti-CD8 (BD Pharmingen) and PE-conjugated recombinant soluble dimeric $H\text{-}2L^d$/Ig fusion protein (BD Pharmingen) complexed with the immunodominant $H\text{-}2L^d$-restricted HBs envelope 28–39 peptide ($HBs^{28–39}$) as described by Isogawa et al. (9). The in vivo cytotoxicity assay was carried out as described (6). Briefly, spleen cells from naive B10D2 mice were stained with carboxyfluorescein diacetate succinimidyl ester (CFSE; Invitrogen) at a concentration of 3 μM ($CFSE^{hi}$) or 0.3 μM ($CFSE^{lo}$). The $CFSE^{hi}$ cells were coated with $HBs^{28–39}$ (1 μM), and the $CFSE^{lo}$ cells were coated with an irrelevant lymphocytic choriomeningitis virus (LCMV)-derived peptide ($NP^{118–126}$). After extensive washing, equal numbers of the $CFSE^{hi}$ and $CFSE^{lo}$ cells (10^7 cells per mouse) were mixed and i.v. injected into groups of Ctrl B10D2 mice or into groups of lineage 107-5 TG mice that had been reconstituted with an HBsAg-primed NT immune system and had been treated either with diluents (Vehicle) or with aspirin (Asp), clopidogrel (Clo), or both (Asp/Clo) starting 60 or 150 d earlier. Mice were killed 16 h after injection, and IHLs were isolated as above. Gating on leukocytes, the percentage of killing was calculated as follows: 100 − {[(% $CFSE^{hi}$-coated cells in 107-5 mice/% $CFSE^{lo}$ cells in 107-5 mice)/(% $CFSE^{hi}$-coated cells in B10D2 mice/% $CFSE^{lo}$ cells in B10D2 mice)] × 100}.

Analyses by MRI. Live 107-5 mice and explanted whole livers were subjected to MRI analyses to (*i*) diagnose HCC, (*ii*) determine HCC volume, and (*iii*) generate 3D liver reconstructions. All MRI analyses were performed using a horizontal 30-cm-bore 7-T magnetic resonance scanner (BioSpec 70/30 USR, Paravision 5.0; Bruker) equipped with a gradient system characterized by an amplitude of 450/675 mT/m, a slew rate of 3,400/4,500 T·m·s, and

a rise time of 140 ms, coupled with a dedicated four-channel mouse body coil. In vivo MRI analyses were carried out in mice under general anesthesia with isoflurane [5% (vol/vol) for induction and 2% (vol/vol) for maintenance] in oxygen at a rate of 2 L/min through a nose cone. During acquisition, mice were positioned prone on a dedicated temperature control apparatus to prevent hypothermia. Breathing and body temperature were continuously monitored during MRI (SA Instruments, Inc.). MRI analyses included the acquisition of transverse liver T2-weighted (T2w) and T1- weighted (T1w) images before and after i.v. administration of gadoxetic acid (35 mg/g of body weight, Primovist; Bayer Schering Pharma) as basically described (10). The specific sequence parameters for T2w or T1w acquisition, respectively, were as follows: T2w [Turbo rapid acquisition relaxation enhanced (TurboRARE)-T2 sequence]: repetition time (TR) = 2744 ms, echo time (TE) = 33 ms, voxel size = 0.097 × 0.117 × 0.8 mm, number of averages = 4; T1w (RARE-T1 sequence): TR = 866 ms, TE = 8.6 ms, voxel size = 0.089 × 0.136 × 0.8 mm, number of averages = 4. Ex vivo MRI analyses were also performed. Whole livers were fixed in Zn-formalin and embedded in 1% agar gel within 50-mL Falcon tubes. In addition to the T2w and T1w images previously described, a 3D T1w sequence was applied for volume rendering reconstruction. The sequence was carried out with advanced image segmentation software (Mipav Software, 5.3.4 version, National Institutes of Health). A highly experienced radiologist (A.E.), blinded to any other information, manually identified liver lesions based on hypointensity on Primovist-enhanced T1w images and hyperintensity on T2w images on each slice; lesions were selected as a region of interest, and individual volumes (lesion area × slice thickness) in each slice were summed up to define the total HCC mass (calculated as % of total liver mass).

1. Nakamoto Y, Guidotti LG, Kuhlen CV, Fowler P, Chisari FV (1998) Immune pathogenesis of hepatocellular carcinoma. *J Exp Med* 188:341–350.
2. Nakamoto Y, Suda T, Momoi T, Kaneko S (2004) Different procarcinogenic potentials of lymphocyte subsets in a transgenic mouse model of chronic hepatitis B. *Cancer Res* 64:3326–3333.
3. Kakimi K, et al. (2001) Blocking chemokine responsive to gamma-2/interferon (IFN)-gamma inducible protein and monokine induced by IFN-gamma activity in vivo reduces the pathogenetic but not the antiviral potential of hepatitis B virus-specific cytotoxic T lymphocytes. *J Exp Med* 194:1755–1766.
4. Sitia G, et al. (2011) Kupffer cells hasten resolution of liver immunopathology in mouse models of viral hepatitis. *PLoS Pathog* 7:e1002061.
5. Jang JH, et al. (2008) Ischemic preconditioning and intermittent clamping confer protection against ischemic injury in the cirrhotic mouse liver. *Liver Transpl* 14:980–988.
6. Iannacone M, et al. (2008) Platelets prevent IFN-alpha/beta-induced lethal hemorrhage promoting CTL-dependent clearance of lymphocytic choriomeningitis virus. *Proc Natl Acad Sci USA* 105:629–634.
7. Ishak K, et al. (1995) Histological grading and staging of chronic hepatitis. *J Hepatol* 22:696–699.
8. Guidotti LG, Matzke B, Schaller H, Chisari FV (1995) High-level hepatitis B virus replication in transgenic mice. *J Virol* 69:6158–6169.
9. Isogawa M, Furuichi Y, Chisari FV (2005) Oscillating CD8(+) T cell effector functions after antigen recognition in the liver. *Immunity* 23:53–63.
10. Freimuth J, et al. (2010) Application of magnetic resonance imaging in transgenic and chemical mouse models of hepatocellular carcinoma. *Mol Cancer* 9:94.

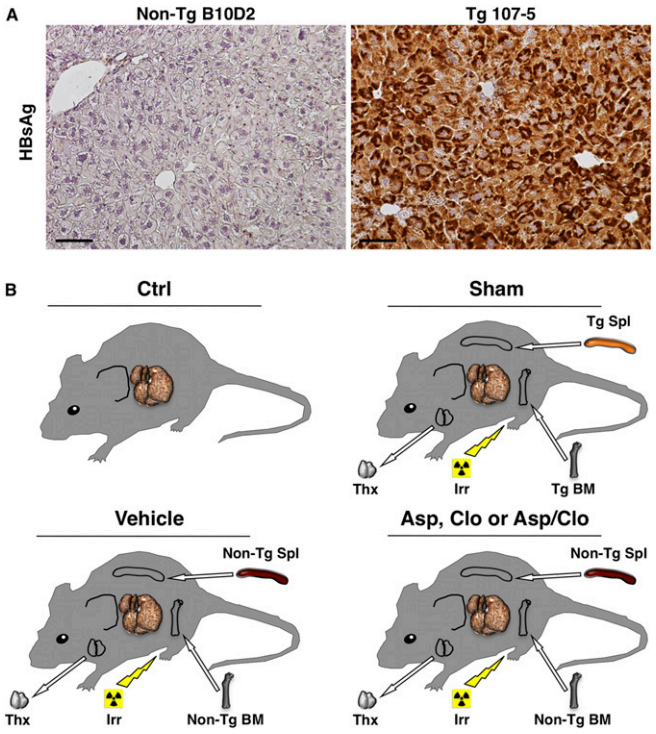

Fig. S1. Liver HBsAg expression in 107-5 TG mice and treatment protocol for the study. (*A*) Micrographs of representative histological liver preparations from NT (*Left*) or TG 107-5 (*Right*) mice are shown. HBsAg is shown in brown. (Scale bars = 50 μm.) (*B*) Animals from the Ctrl group remained unmanipulated for the entire study. Animals from the Sham-treated group underwent thymectomy (Thx) and irradiation (Irr) before being infused with BM and spleen cells from immunologically tolerant TG littermates. Animals from the Vehicle-, Asp-, Clo-, or Asp/Clo-treated group underwent Thx and Irr before being infused with BM and HBsAg-primed spleen cells from B10D2 NT (Non-Tg) mice; these animals were then treated with diluent, Asp, Clo, or the two drugs combined, respectively (Fig. S2).

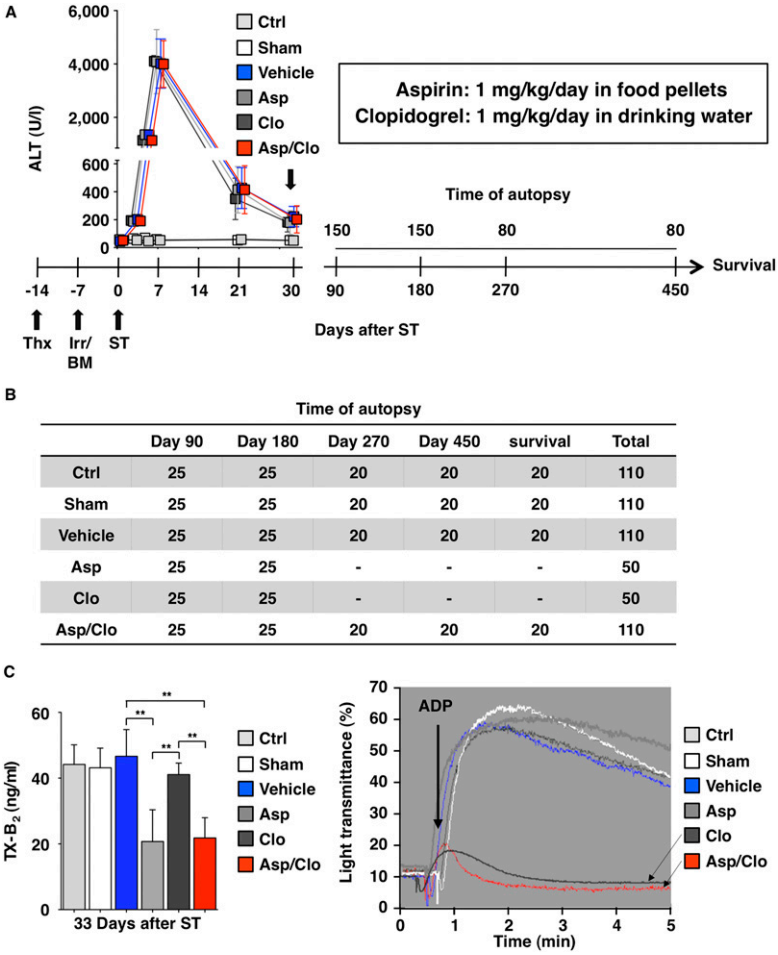

Fig. S2. Study design and platelet response to Asp, Clo, or Asp/Clo treatment. (*A*) Mean serum alanine aminotransferase (ALT) activity (U/L ± SD) was measured at the indicated time points in 107-5 mice belonging to the different study groups described in Fig. S1 (20 mice per group per time point). The times of thymectomy (Thx), irradiation (Irr), BM reconstitution, and autopsy are indicated relative to spleen transfer (ST), which is considered time 0. Note that serum ALT activity increased from preinjection values of 30–40 U/L to ∼4,000 U/L by day 7 after the transfer of HBsAg-primed spleen cells. When serum ALT activity dropped to values approximately threefold to fourfold above normal (by day 30), treatment with Vehicle or with Asp and/or Clo (administered orally for a daily intake of ∼1 mg·kg·d each; *Materials and Methods*) was initiated and continued regularly until the time of autopsy. (*B*) Total number of mice that entered the study is indicated and represents the sum of five independent experiments consisting of five mice per group (all groups, $n = 25$) that were killed at day 90 or 180 after ST and four independent experiments consisting of five mice per group (Sham-, Vehicle-, and Asp/Clo-treated groups and Ctrl group) that were killed at day 270 or 450 after ST. Four additional experiments (each consisting of 5 mice from the Ctrl group and the Sham-, Vehicle-, and Asp/Clo-treated groups) monitored survival. (*C*) Mean TX-B_2 serum content (*Left*; ng/mL ± SD, 20 mice per group) and ADP-dependent platelet aggregation of platelet-rich plasma (*Right*; pooled from 5 representative mice per group) in animals from the indicated groups that were bled simultaneously 3 d after antiplatelet treatment initiation. The statistical significance of differences in the assays shown in *C* (*Left*) is indicated (**$P < 0.001$).

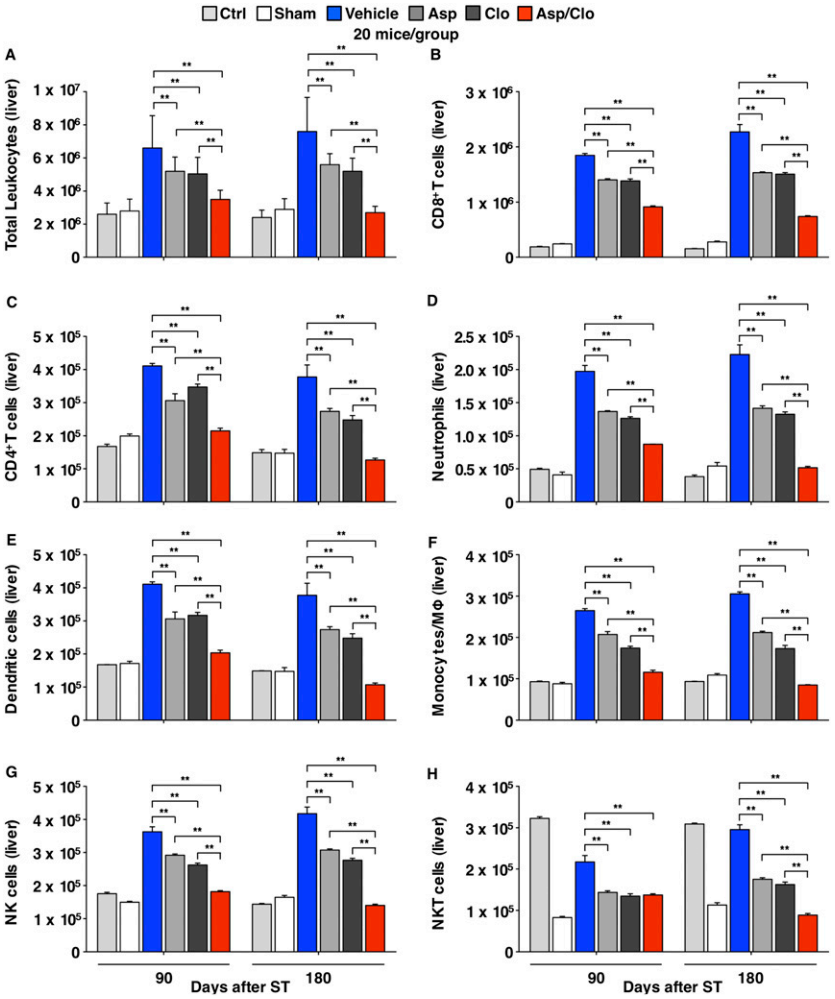

Fig. S3. Treatment with Asp/Clo reduces the hepatic accumulation of antigen-nonspecific inflammatory cells. Absolute numbers of total hepatic leukocytes (*A*), hepatic $CD8^+/TCR^+$ cells ($CD8^+$ T cells) (*B*), hepatic $CD4^+/TCR^+$ cells ($CD4^+$ T cells) (*C*), hepatic $LY6G^+/CD11c^-$ cells (neutrophils) (*D*), hepatic $CD11b^-/CD11c^+$ cells (dendritic cells) (*E*), hepatic $CD11b^+/CD11c^-$ cells (macrophages) (*F*), hepatic $NK1.1^+/CD3^-$ cells (NK cells) (*G*), and hepatic $NK1.1^+/CD3^+$ cells (NKT cells) (*H*) recovered from the liver of the same mice described in Fig. 1 (20 mice per group per time point) are shown. The statistical significance of differences is indicated (**$P < 0.001$).

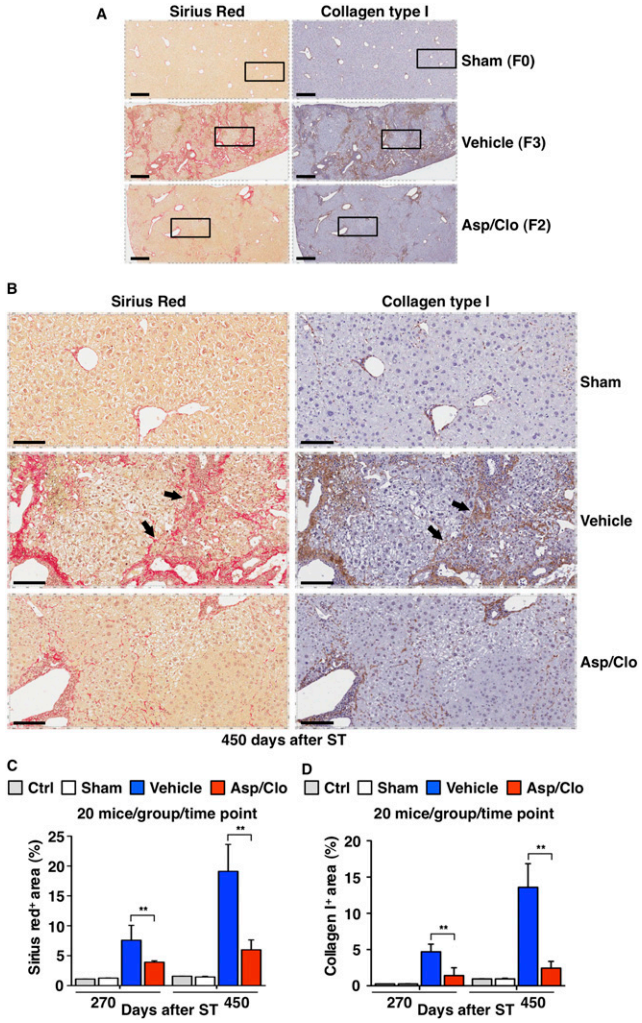

Fig. S4. Treatment with Asp/Clo reduces the severity of liver fibrosis. (*A*) Micrographs of representative histological liver preparations from the indicated groups of mice at day 450 after spleen transfer (ST). (*Insets*) Areas that are shown below at higher magnification. F0, no fibrosis; F2, fibrous expansion of most portal areas with or without short fibrous septa; F3, bridging fibrosis without cirrhosis. (Scale bar = 500 μm.) (*B*) Micrographs of the same histological liver preparations described above at higher magnification. Arrows indicate fibrous septa connecting different portal tracts. (Scale bar = 100 μm.) Sirius Red staining is shown in red (*Left*), and collagen type I staining is shown in brown (*Right*). Collagen deposition (mean % of positive area ± SD; *Materials and Methods*) quantified by either Sirius Red (*C*) or collagen type I (*D*) staining of the same livers described in *A* is shown. Compared with Ctrl or Sham-treated mice killed at day 270 or 450, Vehicle- or Asp/Clo-treated mice showed levels of collagen deposition that were ∼fivefold and ∼15-fold or ∼twofold and ∼threefold higher, respectively. The statistical significance of differences in the assays shown in *C* and *D* is indicated (**$P < 0.001$).

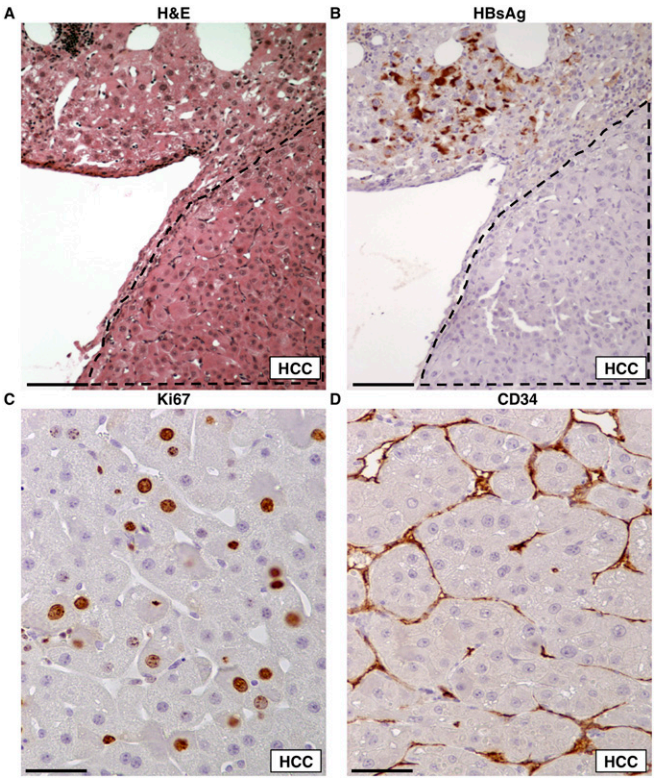

Fig. S5. Histological features of well-differentiated HCCs in Vehicle-treated mice. Micrographs of a representative liver from Vehicle-treated mice killed at day 450 after spleen transfer (ST) are shown. H&E (*A*) or HBsAg (*B*) staining on consecutive sections is shown. Dashed lines demarcate an encapsulated HCC characterized by trabecular cords of neoplastic hepatocytes that were not infiltrated by inflammatory cells and expressed no HBsAg (in contrast to hepatocytes from the noncancerous liver parenchyma above). Note that similar histological features were observed in the less frequent and usually smaller HCCs detected in Asp/Clo-treated mice. (Scale bar = 100 μm.) Ki67 (*C*) or CD34 (*D*) staining of a representative large HCC (>7 mm in diameter) detected in Vehicle-treated mice killed at day 450 after ST is shown. (Scale bar = 50 μm.) HBsAg, Ki67, and CD34 are shown in brown.

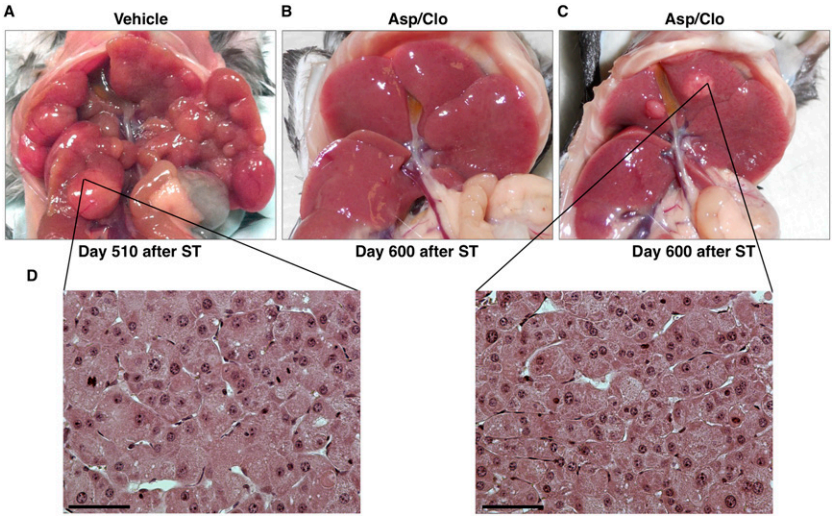

Fig. S6. Gross liver appearance and HCC histology in Vehicle- or Asp/Clo-treated mice at late time points. Photographs depict the gross liver appearance of representative Vehicle- (*A*) or Asp/Clo- (*B* and *C*) treated mice examined at day 510 or 600 after spleen transfer (ST), respectively. Note that the livers shown in *B* and *C* represent the two extreme outcomes of immune-mediated liver injury in Asp/Clo-treated mice: absence of HCC (*B*) or presence of few and small lesions (*C*). (*D*) Micrographs display the histological appearance of the indicated HCCs. H&E staining. (Scale bar = 50 μm.)

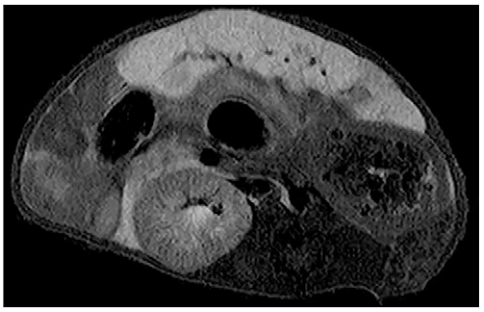

Movie S1. Twenty-four consecutive T1w slices encompassing the whole liver (in a caudal-to-cranial direction) of the Vehicle-treated mouse described in Fig. 4*A, Left*, are shown. The red arrows indicate hypointense regions identifying HCCs.

Movie S1

Movie S2. Twenty-four consecutive T1w slices encompassing the whole liver (in a caudal-to-cranial direction) of the Asp/Clo-treated mouse described in Fig. 4*A, Right*, are shown. The red arrows indicate hypointense regions identifying HCCs.

Movie S2

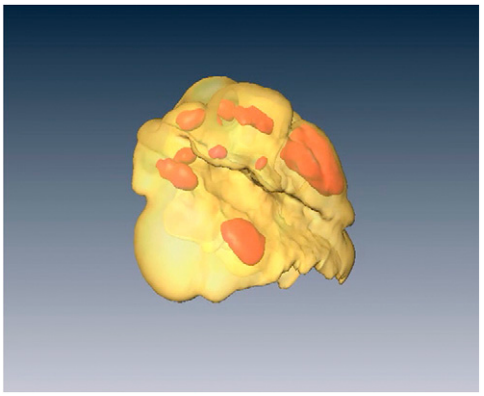

Movie S3. Rotating 3D liver reconstruction of the same Vehicle-treated mouse described in Movie S1 is shown. HCCs are depicted in orange-red.

Movie S3

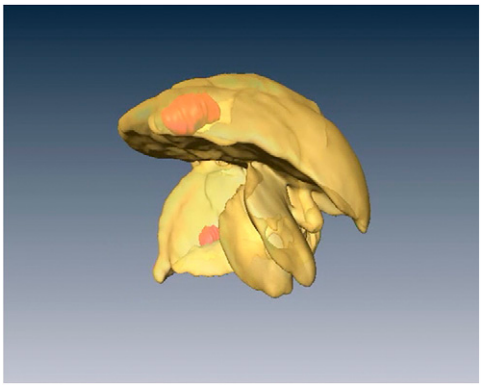

Movie S4. Rotating 3D liver reconstruction of the same Asp/Clo-treated mouse described in Movie S2 is shown. HCCs are depicted in orange-red.

Movie S4